THE ASTROPHYSICAL JOURNAL, 503:717–728, 1998 August 20
© 1998. The American Astronomical Society. All rights reserved. Printed in U.S.A.

ABUNDANCES OF HCN AND HNC IN DARK CLOUD CORES

TOMOYA HIROTA AND SATOSHI YAMAMOTO
Department of Physics and Research Center for the Early Universe, University of Tokyo, Bunkyo-ku, Tokyo, 113-0033, Japan;
hirota@taurus.phys.s.u-tokyo.ac.jp

AND

HITOMI MIKAMI AND MASATOSHI OHISHI[1]
Nobeyama Radio Observatory, Nobeyama, Minamimaki-mura, Minamisaku-gun, Nagano, 384-1305, Japan
Received 1998 January 13; accepted 1998 March 27

ABSTRACT

We have determined the abundances of HCN and HNC toward 19 nearby dark cloud cores by observations of optically thin $H^{13}CN$ ($J = 1$–0) and $HN^{13}C$ ($J = 1$–0) lines. The column density of HCN is found to be correlated with that of HNC. The abundance ratio of [HNC]/[HCN] is determined to be 0.54–4.5 in the observed dark cloud cores. These results are consistent with the idea that HCN and HNC are produced mainly by a recombination reaction of $HCNH^+$ with electrons in dark cloud cores. Furthermore, the [HNC]/[HCN] ratio does not show any significant differences between star-forming cores and starless cores. The HCN and HNC abundances are compared with those for the OMC-1 cores previously reported. Although the abundances of HCN in the OMC-1 cores are comparable to those in the dark cloud cores, the abundances of HNC in OMC-1 are 1–2 orders of magnitude less than those in dark cloud cores. It is suggested that HNC is destroyed by neutral-neutral reactions in high kinetic temperature regions.

Subject headings: ISM: abundances — ISM: molecules — molecular processes — radio lines: ISM

1. INTRODUCTION

Hydrogen cyanide, HCN, is one of the most basic interstellar molecules, and its spectral lines are observed in many Galactic and extragalactic objects. The HCN molecule has a large electric dipole moment, 2.985 ± 0.005 debye (Bhattacharya & Gordy 1960), so that the critical density for the $J = 1$–0 transition is as high as 10^6 cm^{-3}. Therefore, the HCN lines are used as good tracers of dense gas in molecular clouds.

Hydrogen isocyanide, HNC, is a geometrical isomer of HCN, and its spectral lines are also observed in many interstellar clouds. Since HNC is higher in energy and therefore less stable than HCN by 3920 cm^{-1} (Bentley, Huang, & Wyatt 1993), the equilibrium ratio of [HNC]/[HCN] is calculated to be less than 10^{-25} in interstellar clouds, where the kinetic temperatures are lower than 100 K. However, the [HNC]/[HCN] ratio in interstellar clouds is known to be much higher than this equilibrium value, reflecting the production and isomerization mechanisms of these two species.

HCN and HNC are thought to be among the reactants for production reactions of cyanopolyynes ($HC_{2n+1}N$), which are also abundant in dark cloud cores. Especially in early stages of evolution, the abundances of carbon chain molecules such as C_nS and $HC_{2n+1}N$ in dark cloud cores are known to be enhanced (Suzuki et al. 1992). According to pseudo–time-dependent models, both HCN and HNC are enhanced in the early phase, whereas their abundances decline toward steady state (Lee, Bettens, & Herbst 1996). Therefore, observations of HCN and HNC are also important for understanding the chemical evolution of dark cloud cores. Critical comparison of the observed abundances with those derived from the model calculations would be a good test of the proposed production scheme.

The [HNC]/[HCN] abundance ratio (hereafter the HNC/HCN ratio) in a typical giant molecular cloud, OMC-1, is well studied so far (Goldsmith et al. 1981, 1986; Schilke et al. 1992). It is found that the HNC/HCN ratio in the OMC-1 ridge ranges from 1 to 1/90 and that the HNC/HCN ratio is especially low in hot core regions around the Kleinmann-Low object (Schilke et al. 1992). Recently, similar results were obtained by Ungerechts et al. (1997) also.

In contrast to these results, the HNC/HCN ratio in dark cloud cores has been reported to be on the order of unity. For example, Irvine & Schloerb (1984) observed $H^{13}CN$, $HN^{13}C$, $HC^{15}N$, and $H^{15}NC$ in TMC-1 and determined the HNC/HCN ratio to be 1.55 ± 0.16. In L134N, another well-studied dark cloud core, the HNC/HCN ratios were found to be 2.5 ± 1.1, 1.3 ± 0.6, and 1.7 ± 2.9 at three different positions by observations of $H^{13}CN$ and $HN^{13}C$ (Swade 1989a, 1989b). However, the abundances of HCN and HNC are poorly known for other dark cloud cores. Churchwell, Nash, & Walmsley (1984) observed $H^{13}CN$ and $HN^{13}C$ in several dark cloud cores, including TMC-1 and L134N, and in two warm clouds with H II regions. Since $H^{13}CN$ was not detected in their observations, they estimated the HNC/HCN ratios to be 3–10 by using the upper limit of $H^{13}CN$ and the lower limit of $H^{12}CN$. Harju (1989) determined the $HN^{12}C/H^{12}CN$ intensity ratio to be on the order of unity in 23 dark cloud cores. However, the results may contain large uncertainties, because $H^{12}CN$ and $HN^{12}C$ are known to be strongly self-absorbed (e.g., Irvine & Schloerb 1984; Churchwell et al. 1984). Therefore, abundances of HCN and HNC in dark cloud cores are not known with sufficient accuracy except for TMC-1 and L134N.

Considering the importance of the HCN and HNC lines

[1] Present address: National Astronomical Observatory, 2-21-1 Osawa, Mitaka, Tokyo 181-8588, Japan.

TABLE 1

OBSERVED LINES

Molecule	Transition	ν (MHz)	μ (D)	S_{ul}[a]
$H^{12}CN$.....	$J = 1–0$, $F = 1–1$	88630.42	2.985[b]	1.000
	$F = 2–1$	88631.85		1.667
	$F = 0–1$	88633.94		0.333
$H^{13}CN$.....	$J = 1–0$, $F = 1–1$	86338.77	2.985[b]	1.000
	$F = 2–1$	86340.18		1.667
	$F = 0–1$	86342.27		0.333
$HN^{13}C$.....	$J = 1–0$	87090.85	3.05[c]	1.000

[a] Intrinsic line strength including hyperfine splitting.
[b] Bhattacharya & Gordy 1960.
[c] Blackman et al. 1976.

in astrophysical and astrochemical studies, it is of fundamental significance to determine the HCN and HNC abundances in dark cloud cores accurately. On the basis of this motivation, we observed the spectra of $H^{13}CN$ and $HN^{13}C$ toward 19 dark cloud cores with various physical conditions.

2. OBSERVATIONS

Observations were made in 1992 April with the 45 m radio telescope of Nobeyama Radio Observatory. We observed the $J = 1–0$ transitions of $H^{12}CN$, $H^{13}CN$, and $HN^{13}C$. The $H^{13}CN$ and $HN^{13}C$ lines were simultaneously observed with two different receivers by using the polarization beam splitter. Their rest frequencies, dipole moments, and intrinsic line strengths are summarized in Table 1.

We used two SIS mixer receivers, whose single-sideband system temperatures were 300–550 K (typically about 350 K) including atmospheric attenuation. One SIS mixer receiver is for observations of $H^{13}CN$, and the other is for observations of $HN^{13}C$. The beam size was 20″ (half-power beamwidth [HPBW]), and the beam efficiency was 0.5. These values are provided by the observatory on the basis of observations of planets. This beam size and the efficiency were almost the same for the two receivers. Eight acousto-optical radio spectrometers were used as the back end. The spectral resolution was 37 kHz, which corresponds to a velocity resolution of 0.13 km s^{-1} in the 86–88 GHz region. Pointing was checked by observing nearby SiO maser sources every 2 hours, and the pointing accuracy was estimated to be 5″ (rms). All the observations were performed with the position-switching mode, in which a typical off position was 10′ away from the source position in right ascension. The on-source integration time was 5–30 minutes for each source, which resulted in rms noise temperatures of 0.04–0.16 K.

We observed 19 nearby dark cloud cores: 12 are in the Taurus region, four in the Ophiuchus region, and three in other regions, as summarized in Table 2. The coordinates of the observed positions are mainly from Myers, Linke, & Benson (1983) and Suzuki et al. (1992). Only one position in each cloud core was observed. We observed nine star-forming cores, which are associated with *IRAS* sources and molecular outflows, and 10 starless cores.

3. RESULTS

3.1. *Observed Spectra and Line Parameters*

Observed line parameters are summarized in Table 3, and a few examples of observed spectra are shown in Figure 1. When the peak antenna temperature at the expected velocity is larger than 3 times the rms noise temperature, we judged that the line is detected. Based on this criterion, $H^{12}CN$, $H^{13}CN$, and $HN^{13}C$ were detected in 19, 12, and 17 cores, respectively. The $H^{12}CN$ ($J = 1–0$) and $H^{13}CN$ ($J = 1–0$) spectra consist of three hyperfine components caused by the nuclear spin of the nitrogen nucleus ($I = 1$). In optically thin and LTE conditions, the relative intensity of these three hyperfine components of the $J = 1–0$ transitions is 5:3:1 for $F = 2–1$, $F = 1–1$, and $F = 0–1$, respec-

TABLE 2

OBSERVED DARK CLOUD CORES

Source Name	α(1950.0)	δ(1950.0)	Distance (pc)	$N(H_2)$ (10^{22} cm^{-2})	*IRAS* Number	Outflow Reference
B1	03 30 10.5	30 57 47	350	0.94	03301+3057	1
L1489	04 01 48.1	26 10 21	140	0.67	04016+2610	2
L1498	04 07 50.0	25 02 13	140	0.46	...	
L1495B	04 12 30.0	28 39 39	140	1.2	...	
L1521B	04 21 08.5	26 30 00	140	1.8	...	
L1521E	04 26 12.5	26 07 17	140	1.1	...	
L1551	04 28 40.0	18 01 42	140	0.98	04287+1801	3
TMC-2.....	04 29 43.0	24 18 15	140	0.94	...	
L1527	04 36 49.3	25 57 16	140	...	04368+2557	4
TMC-1(NH_3)[a].....	04 38 14.5	25 42 30	140	0.85	04381+2540	4
TMC-1C.....	04 38 28.0	25 55 00	140	1.2	...	
TMC-1[b]	04 38 38.6	25 35 45	140	3.1	...	
L1544	05 01 11.1	25 07 40	140	1.3	...	
Lup-1	15 39 51.2	−33 59 36	150	...	15398−3359	5
L134N(L183).....	15 51 24.0	−02 43 00	150	0.86	...	
L1709B	16 28 38.4	−23 55 00	160	1.7	16285−2356	6
L1689N	16 29 27.6	−24 21 53	160	3.1	16293−2422	7
L43E	16 31 48.5	−15 40 33	160	0.92	16316−1540	2
L63.....	16 47 21.0	−18 01 00	160	0.46	...	

NOTE.—Units of right ascension are hours, minutes, and seconds, and units of declination are degrees, arcminutes, and arcseconds.
[a] Ammonia peak.
[b] Cyanopolyyne peak.
REFERENCES.—(1) Bachiller et al. 1990; (2) Myers et al. 1988; (3) Snell et al. 1980; (4) Heyer et al. 1987; (5) Tachihara et al. 1996; (6) Parker et al. 1991; (7) Fukui et al. 1986.

TABLE 3

OBSERVED LINE PARAMETERS

Source Name	Molecule	Transition	T_A^* (K)	T_{rms} (K)	v_{LSR} (km s^{-1})	Δv (km s^{-1})	$\int T_A^* dv$ (K km s^{-1})	Note
B1	$H^{12}CN$	$F = 2–1$	1.07	0.087	5.43	1.37	2.19	a
		$F = 1–1$	0.75		5.92	1.24	1.39	
		$F = 0–1$	0.77		5.98	1.00	1.12	
	$H^{13}CN$	$F = 2–1$	0.23	0.042	6.14	1.06	0.23	
		$F = 1–1$	0.19		6.10	0.50	0.14	
		$F = 0–1$	<0.13		...	...	...	b
	$HN^{13}C$		0.44	0.058	6.11	0.76	0.45	
L1489	$H^{12}CN$	$F = 2–1$	1.63	0.161	5.42	0.69	1.04	
		$F = 1–1$	1.07		5.96	0.50	0.59	
		$F = 0–1$	0.90		5.97	0.43	0.52	
	$H^{13}CN$	$F = 2–1$	0.11	0.040	6.85	0.36	0.03	
		$F = 1–1$	0.15		6.74	0.55	0.09	
		$F = 0–1$	<0.12		...	...	...	b
	$HN^{13}C$		0.32	0.044	6.62	0.51	0.22	
L1498	$H^{13}CN$	$F = 2–1$	0.14	0.044	7.84	0.35	0.05	
		$F = 1–1$	<0.13		...	...	...	b
		$F = 0–1$	<0.13		...	...	...	b
	$HN^{13}C$		0.60	0.045	7.99	0.55	0.35	
L1495B	$H^{13}CN$	$F = 2–1$	<0.12	0.040	...	...	...	b
		$F = 1–1$	<0.12		...	...	...	b
		$F = 0–1$	<0.12		...	...	...	b
	$HN^{13}C$		0.20	0.051	7.65	0.37	0.08	
L1521B	$H^{12}CN$	$F = 2–1$	0.42	0.169	6.45	0.25	0.21	
		$F = 1–1$	0.54		6.18	0.23	0.13	
		$F = 0–1$	0.44		6.31	0.38	0.18	
	$H^{13}CN$	$F = 2–1$	0.15	0.054	6.60	0.32	0.07	
		$F = 1–1$	<0.16		...	...	...	b
		$F = 0–1$	<0.16		...	...	...	b
	$HN^{13}C$		0.39	0.060	7.08	0.42	0.19	
L1521E	$H^{12}CN$	$F = 2–1$	0.86	0.097	6.99	0.82	0.66	a
		$F = 1–1$	0.56		6.99	0.82	0.38	a
		$F = 0–1$	0.68		6.67	0.65	0.42	
	$H^{13}CN$	$F = 2–1$	0.25	0.047	6.93	0.58	0.15	
		$F = 1–1$	0.16		6.82	0.43	0.05	
		$F = 0–1$	<0.14		...	...	...	b
	$HN^{13}C$		0.32	0.053	6.71	0.44	0.15	
L1551	$H^{12}CN$	$F = 2–1$	1.65	0.097	6.14	0.45	1.69	a
		$F = 1–1$	1.34		6.21	0.99	1.22	a
		$F = 0–1$	1.16		6.27	0.72	0.98	
	$H^{13}CN$	$F = 2–1$	<0.14	0.048	...	...	...	b
		$F = 1–1$	<0.14		...	...	...	b
		$F = 0–1$	<0.14		...	...	...	b
	$HN^{13}C$		0.20	0.056	6.33	0.44	0.15	
TMC-2.....	$H^{13}CN$	$F = 2–1$	0.16	0.044	6.32	0.44	0.08	
		$F = 1–1$	<0.13		...	...	...	b
		$F = 0–1$	<0.13		...	...	...	b
	$HN^{13}C$		0.49	0.045	6.24	0.57	0.29	
L1527	$H^{12}CN$	$F = 2–1$	1.36	0.065	5.52	0.49	1.23	
		$F = 1–1$	0.89		5.55	0.48	0.54	
		$F = 0–1$	0.71		5.62	0.62	0.41	
	$H^{13}CN$	$F = 2–1$	0.15	0.042	6.12	0.61	0.08	
		$F = 1–1$	<0.13		...	...	...	b
		$F = 0–1$	<0.13		...	...	...	b
	$HN^{13}C$		0.29	0.045	5.75	0.57	0.16	
TMC-1 (NH_3).....	$H^{13}CN$	$F = 2–1$	0.24	0.046	5.96	0.51	0.13	
		$F = 1–1$	0.15		5.78	0.44	0.08	
		$F = 0–1$	<0.14		...	...	...	b
	$HN^{13}C$		0.59	0.052	5.82	0.85	0.49	
TMC-1C.....	$H^{13}CN$	$F = 2–1$	<0.14	0.043	...	...	...	b
		$F = 1–1$	<0.14		...	...	...	b
		$F = 0–1$	<0.14		...	...	...	b
	$HN^{13}C$		0.25	0.050	5.33	0.36	0.12	
TMC-1.....	$H^{12}CN$	$F = 2–1$	0.19	0.081	5.48	0.24	0.13	
		$F = 1–1$	0.42		5.41	0.31	0.33	
		$F = 0–1$	0.96		5.75	0.67	0.62	
	$H^{13}CN$	$F = 2–1$	0.25	0.038	5.77	0.63	0.18	
		$F = 1–1$	0.21		6.03	0.76	0.15	
		$F = 0–1$	0.14		5.77	0.50	0.06	
	$HN^{13}C$		0.59	0.060	5.89	0.82	0.46	

TABLE 3—*Continued*

Source Name	Molecule	Transition	T_A^* (K)	T_{rms} (K)	v_{LSR} (km s^{-1})	Δv (km s^{-1})	$\int T_A^* dv$ (K km s^{-1})	Note
L1544	$H^{12}CN$	$F = 2–1$	1.31	0.071	6.81	0.35	0.57	
		$F = 1–1$	0.66		6.83	0.39	0.27	
		$F = 0–1$	0.80		6.90	0.34	0.31	
	$H^{13}CN$	$F = 2–1$	<0.14	0.048	...	...	...	b
		$F = 1–1$	<0.14		...	...	...	b
		$F = 0–1$	<0.14		...	...	...	b
	$HN^{13}C$		0.43	0.055	7.19	0.70	0.34	
Lup-1	$H^{12}CN$	$F = 2–1$	0.71	0.082	4.92	0.45	0.45	
		$F = 1–1$	0.57		4.98	0.43	0.34	
		$F = 0–1$	0.79		5.00	0.51	0.51	
	$H^{13}CN$	$F = 2–1$	0.25	0.099	5.29	0.55	0.15	
		$F = 1–1$	0.36		5.25	0.51	0.19	
		$F = 0–1$	<0.30		...	...	...	b
	$HN^{13}C$		1.03	0.129	5.21	0.66	0.63	
L134N	$H^{12}CN$	$F = 2–1$	0.41	0.056	3.00	0.64	0.22	
		$F = 1–1$	0.21		3.17	0.79	0.16	
		$F = 0–1$	0.18		2.33	0.43	0.12	
	$H^{13}CN$	$F = 2–1$	0.13	0.044	2.90	0.40	0.03	
		$F = 1–1$	<0.13		...	...	...	b
		$F = 0–1$	<0.13		...	...	...	b
	$HN^{13}C$		<0.19	0.062	...	...	...	
L1709B	$H^{12}CN$	$F = 2–1$	0.54	0.105	2.94	0.33	0.18	a
		$F = 1–1$	0.20		3.15	0.31	0.04	a
		$F = 0–1$	0.40		3.00	0.30	0.22	
	$H^{13}CN$	$F = 2–1$	<0.14	0.049	...	...	...	b
		$F = 1–1$	<0.14		...	...	...	b
		$F = 0–1$	<0.14		...	...	...	b
	$HN^{13}C$		<0.20	0.068	...	...	...	b
L1689N	$H^{12}CN$	$F = 2–1$	1.03	0.072	3.20	0.69	1.71	a
		$F = 1–1$	0.57		3.27	0.65	1.04	a
		$F = 0–1$	0.45		3.41	0.49	0.37	a
	$H^{13}CN$	$F = 2–1$	0.22	0.041	4.05	0.74	0.22	
		$F = 1–1$	0.19		4.01	0.40	0.12	
		$F = 0–1$	<0.12		...	...	...	b
	$HN^{13}C$		0.63	0.057	3.73	0.85	0.64	
L43E	$H^{12}CN$	$F = 2–1$	0.89	0.081	1.07	0.35	0.57	a
		$F = 1–1$	0.51		1.03	0.36	0.25	a
		$F = 0–1$	0.47		0.89	0.77	0.34	
	$H^{13}CN$	$F = 2–1$	<0.13	0.044	...	...	...	b
		$F = 1–1$	<0.13		...	...	...	b
		$F = 0–1$	<0.13		...	...	...	b
	$HN^{13}C$		0.30	0.062	0.93	0.44	0.13	
L63	$H^{12}CN$	$F = 2–1$	0.61	0.073	5.53	0.99	0.48	
		$F = 1–1$	0.42		5.46	0.35	0.37	
		$F = 0–1$	0.52		5.66	0.26	0.17	
	$H^{13}CN$	$F = 2–1$	<0.20	0.065	...	...	...	b
		$F = 1–1$	<0.20		...	...	...	b
		$F = 0–1$	<0.20		...	...	...	b
	$HN^{13}C$		0.50	0.065	5.85	0.51	0.29	

NOTE.—In the last column the letter "a" indicates lines that have two distinct peaks due to self-absorption; parameters only for the higher peak are given. The letter "b" means not detected. The upper limit is given with 3 σ confidence.

tively. On the other hand, the hyperfine splitting of the $HN^{13}C$ spectrum is about 0.1 MHz (Lovas, Snyder, & Johnson 1979), which is too small to be resolved.

The $H^{12}CN$ lines of L1521E shown in Figure 1 have double-peaked line profiles. A similar double-peaked line profile appears in some other sources noted in Table 3. In TMC-1, the strongest hyperfine component of $H^{12}CN$ ($F = 2–1$) is not seen, as was pointed out by Irvine & Schloerb (1984). Such an anomaly is found only in the $H^{12}CN$ lines. Since the velocity of the dips of $H^{12}CN$ is almost the same as the peak velocity of $H^{13}CN$ and $HN^{13}C$ emission, it is likely that the $H^{12}CN$ lines are strongly self-absorbed even for the weakest hyperfine component ($F = 0–1$). Such an effect of self-absorption is also seen in the $H^{12}CN$ spectra observed toward L1527 and L1544, whose peak velocities are 0.2–0.4 km s^{-1} blueshifted and whose line widths are narrower compared with those of $H^{13}CN$ and $HN^{13}C$ by 0.1–0.3 km s^{-1}. It is suggested that this is evidence of gravitational infall motion (Myers et al. 1995, 1996). Therefore, it is indispensable to observe optically thin lines such as $H^{13}CN$ and $HN^{13}C$ in order to determine the column densities of HCN and HNC accurately.

3.2. *Column Densities of* $H^{13}CN$ *and* $HN^{13}C$

We derived the column densities of $H^{13}CN$ and $HN^{13}C$ using the large velocity gradient (LVG) model (Goldreich & Kwan 1974). We adopted the collision rate for HCN calculated by Monteiro & Stutzki (1986), where the rates between hyperfine sublevels by collision with He atoms are tabulated up to $J = 4$. Since the collision rates for HNC are not known, we used those between HCN and He calculated by Green & Thaddeus (1974). We neglected the hyperfine

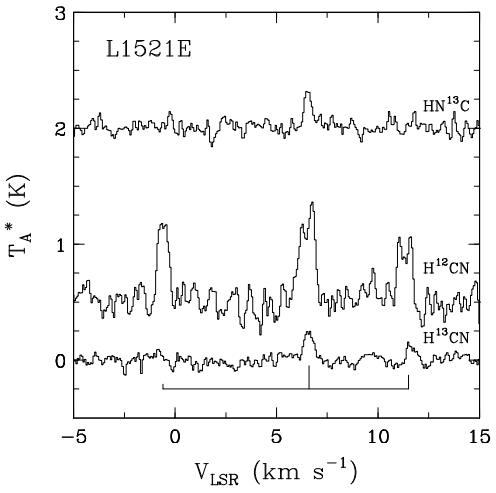

FIG. 1*a*

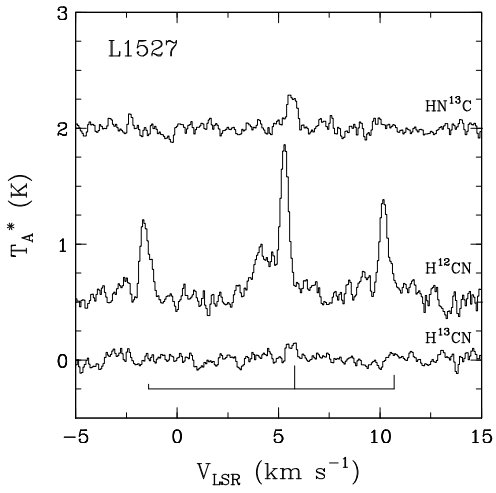

FIG. 1*b*

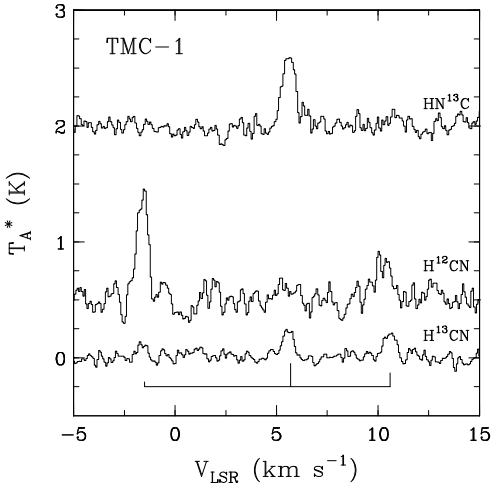

FIG. 1*c*

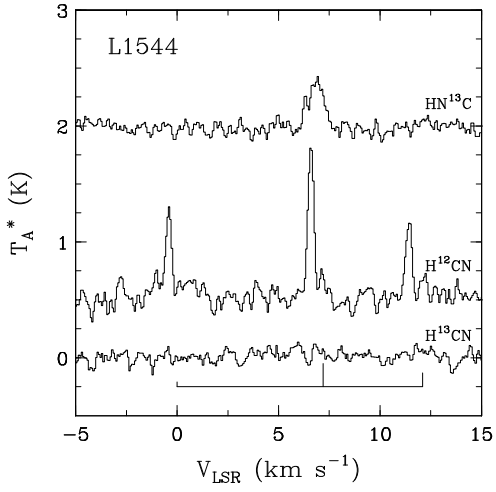

FIG. 1*d*

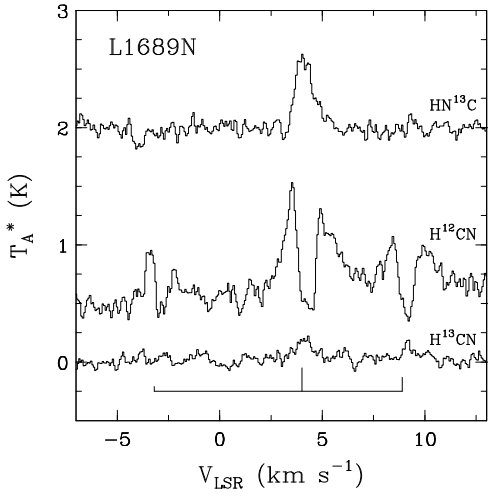

FIG. 1*e*

FIG. 1.—Spectra of $H^{12}CN$, $H^{13}CN$, and $HN^{13}C$ obtained toward (*a*) L1521E , (*b*) L1527, (*c*) TMC-1 , (*d*) L1544 , and (*e*) L1689N. Positions are given in Table 2. A solid line below the spectra indicates the positions and the relative intensities of the hyperfine components of the $H^{13}CN$ lines. The positions of the hyperfine components of $H^{12}CN$ are almost identical to those of $H^{13}CN$ within 0.1 km s^{-1}.

splittings of HNC in the following analysis since they are smaller than the observed line widths. We multiplied the collision rates by a factor of 1.37 to account for the difference in the reduced mass between the He-HCN and para–H_2-HCN systems. The difference in the reduced mass of the isotopic species was also corrected. These corrections are reasonable, as reported in the He-CO and H_2-CO systems (Schinke et al. 1985). Furthermore, the collision rates for the ortho–H_2-HCN and ortho–H_2-HNC systems were assumed to be the same as that for the para–H_2-HCN system.

The kinetic temperatures in dark cloud cores are 8–15 K as observed by the NH_3 and CO lines (Benson & Myers 1989). Therefore, we assumed that the kinetic temperatures in the observed dark cloud cores are 10 K. The H_2 densities derived from the $C^{34}S$ ($J = 2$–1 and 1–0) observations are employed in the analysis (Appendix A). As the $C^{34}S$ data are not available for several cores, we assumed their H_2 density to be 1.0×10^5 cm^{-3}, which is a typical value derived from the $C^{34}S$ observations. For TMC-1C and L134N, the H_2 densities are assumed to be 1.0×10^5 cm^{-3}, since the densities derived from $C^{34}S$ observations are much lower than the critical density of the HCN and HNC $J = 1$–0 lines. The line widths of $H^{13}CN$ and $HN^{13}C$ were used to estimate velocity gradients in the LVG calculations. When these lines were not detected, the line widths of $H^{13}CO^+$ were used to evaluate the upper limits to the column densities. In our observations the spatial resolution was about 0.01–0.03 pc, which is smaller than the emission regions of the HCN and HNC $J = 1$–0 lines in previously observed dark cloud cores (Harju 1989). Thus, we assumed that the source filling factor is unity for all the sources. The errors caused by uncertainties of the assumed parameters such as T_k, $n(H_2)$, and Δv are estimated to be less than a factor of 2.

Column densities of $H^{13}CN$ and $HN^{13}C$ obtained by the LVG calculations are summarized in Table 4 and are plotted in Figure 2. Errors were estimated from the rms noise temperatures of the observed spectra. An error in the line width was ignored. When $H^{13}CN$ and $HN^{13}C$ are not detected, the upper limits are given with 3 σ confidence. For five cores, L1551, L1544, L1709B, L43E, and L63, where the $H^{13}CN$ lines were not detected, the lower limits are calculated from the weakest hyperfine component of $H^{12}CN$ ($F = 0$–1), assuming that the abundance ratio of $^{12}C/^{13}C$ is 60 (Langer & Penzias 1993; Mangum et al. 1988). The averages of the upper and lower limits for the column densities of these five cores are also plotted in Figure 2. According to the LVG calculations, the optical depth of the main hyper-

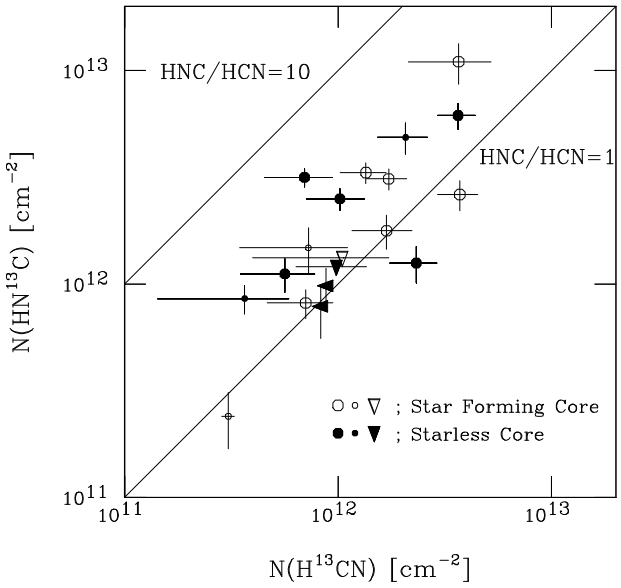

FIG. 2.—Column densities of $H^{13}CN$ and $HN^{13}C$ in dark cloud cores. Open and filled symbols represent the star-forming cores and starless cores, respectively. Error bars correspond to the range of $T_A^* \pm T_{rms}$. The cores where the lower limit of $H^{13}CN$ is determined from the spectra of $H^{12}CN$ are denoted by the small circles. Triangles represent the upper limit of $H^{13}CN$ (or $HN^{13}C$), which is given with 3 σ confidence.

TABLE 4

COLUMN DENSITIES AND FRACTIONAL ABUNDANCES OF HCN AND HNC

Source Name	τ_m ($H^{13}CN$)[a]	N ($H^{13}CN$) (10^{12} cm^{-2})	HCN/H_2[b] (10^{-9})	$\tau(HN^{13}C)$	N ($HN^{13}C$) (10^{12} cm^{-2})	HNC/H_2[b] (10^{-9})	HNC/HCN
B1	0.65	3.7 (8)	24 (5)	1.12	2.6 (4)	17 (3)	0.71 (58)
L1489	0.20	0.71 (24)	4.5 (15)	0.44	0.82 (13)	5.1 (8)	1.2 (3)
L1498	0.39	0.70 (24)	7.3 (25)	1.75	3.2 (3)	33 (3)	4.5 (12)
L1495B	...	<0.83	<4.2	0.84	0.77 (22)	3.9 (11)	>0.93
L1521B	0.32	0.56 (21)	1.9 (7)	0.84	1.1 (2)	3.7 (7)	2.0 (6)
L1521E	0.78	2.3 (6)	13 (3)	1.01	1.3 (2)	6.8 (13)	0.54 (33)
L1551	...	0.29–0.33	1.4–1.6	0.06	0.24 (7)	1.2 (4)	0.73–0.83
TMC-2	0.46	1.0 (3)	5.1 (15)	1.43	2.5 (3)	13 (1)	2.5 (8)
L1527	0.60	1.7 (5)	...	1.20	1.8 (3)	...	1.1 (6)
TMC-1 (NH_3)	0.44	1.3 (3)	9.5 (23)	1.09	3.3 (4)	23 (3)	2.5 (9)
TMC-1C	...	<0.88	<2.9	1.04	0.97 (22)	3.2 (7)	>1.1
TMC-1	1.18	3.7 (7)	7.1 (14)	2.42	6.2 (8)	12 (2)	1.7 (13)
L1544	...	1.5–2.6	7.1–12	2.54	4.9 (8)	22 (4)	1.9–3.3
Lup-1	1.42	3.7 (15)	...	4.23	11 (2)	...	3.0 (46)
L134N	0.54	1.0 (36)	6.3 (23)	...	<1.2	<7.6	<1.2
L1709B	...	0.40–1.7	1.4–6.1	...	<1.3	<4.7	...
L1689N	0.36	1.7 (4)	3.3 (7)	0.94	3.1 (4)	6.0 (7)	1.8 (7)
L43E	...	0.35–1.1	1.9–6.0	1.26	1.5 (4)	8.1 (19)	1.4–4.3
L63	...	0.14–0.59	1.9–7.6	0.27	0.85 (13)	11 (2)	1.5–6.1

NOTE.—The numbers in parentheses represent the errors in unit of the last significant digits. Upper limit is given with 3 σ confidence.

[a] Optical depth for the main hyperfine component ($F = 2$–1).

[b] The $^{12}C/^{13}C$ ratio is assumed to be 60.

fine component ($F = 2$–1) of $H^{13}CN$ is found to be 0.20–1.42, whereas the optical depth of the $HN^{13}C$ line ranges from 0.06 to 4.23. Although the $HN^{13}C$ $J = 1$–0 transitions may be optically thick for several cores, they do not seem to suffer from strong self-absorption. Therefore, the derived $HN^{13}C/H^{13}CN$ ratios are thought to represent the HNC/HCN ratio well. Note that the fraction of the total populations in the $J = 1$ state of $H^{13}CN$ and $HN^{13}C$ are calculated to be 0.45–0.50, and the excitation temperatures for $H^{13}CN$ and $HN^{13}C$ mostly range from 3.5 to 5.0 K.

The calculated column densities of $H^{13}CN$ and the HNC/HCN ratios toward the cyanopolyyne peak of TMC-1 are consistent with those of Irvine & Schloerb (1984) in spite of the difference in beam sizes (20″ for ours and 58″ for Irvine & Schloerb's 1984) and the slight difference in observed positions (33″ north of our observed position). Moreover, the HNC/HCN ratios toward the cyanopolyyne peak and the ammonia peak of TMC-1 obtained by the present study are consistent with those obtained recently by Pratap et al. (1997). Churchwell et al. (1984) reported the HNC/HCN ratios toward TMC-1 (cyanopolyyne peak and ammonia peak), TMC-2, L1544, and L134N, where their observed positions are 40″–2′ away from our positions. Although their results contain large uncertainties because of nondetection of $H^{13}CN$, our results are consistent with theirs.

The HNC/HCN ratio toward the ammonia peak of L1689N observed in the present study is 1.8 ± 0.7. In contrast, van Dishoeck et al. (1995) observed the HNC/HCN ratio by using high-J transitions of 1/12 toward IRAS 16293−2422, which is 100″ west of the ammonia peak. Reasons for this discrepancy arise not only from differences in kinetic temperatures toward the observed positions but also from differences in the observed transitions, as discussed later.

Column densities of $H^{13}CN$ and $HN^{13}C$ show a positive correlation as seen in Figure 2; the correlation coefficient is 0.72. Furthermore, the HNC/HCN ratio ranges from 0.54 to 4.5. The maximum value of the HNC/HCN ratio is 4.5 ± 1.2 in L1498, while the minimum is 0.54 ± 0.33 in L1521E. Although HNC is higher in energy than HCN, its abundance is comparable to that of HCN in dark cloud cores. In the present study, we found that the HNC/HCN ratio does not show any significant differences between star-forming cores and starless cores. Neglecting the cores where either $H^{13}CN$ or $HN^{13}C$ is not detected, we calculated the average HNC/HCN ratio for the star-forming cores and the starless cores. The average HNC/HCN ratio in seven starless cores (excluding L1495B, TMC-1C, and L134N) is 2.5 ± 1.3 (1 σ), whereas that in eight star-forming cores (excluding L1709B) is 1.7 ± 0.9 (1 σ). The average ratio of all the cores except for L1495B, TMC-1C, L134N, and L1709B is 2.1 ± 1.2 (1 σ). The difference between the star-forming cores and the starless cores is smaller than the uncertainty of the abundance ratio in each cloud. These results are in great contrast to the case of OMC-1 (Schilke et al. 1992), where the HNC/HCN ratio varies from 1 to 1/90.

3.3. *The Abundance Ratios of* HCN *and* HNC *Relative to* H_2

The HCN and HNC abundances relative to H_2 are summarized in Table 4 and plotted in Figure 3. The corresponding data for OMC-1 reported by Schilke et al. (1992) are also plotted in Figure 3. The H_2 column densities are from Myers et al. (1983) and Butner, Lada, & Loren (1995), in which the column densities were determined from the $C^{18}O$ observations. For L1489, L1498, L1551, TMC-2, TMC-1C, L134N, and L43E, the H_2 column densities are reported in both papers. We took an average of the two reported values for each source. Differences in the H_2 column densities between these two reports are less than a factor of 3. For B1 and L1689N, the H_2 column densities are from Bachiller et al. (1990) and Loren, Wootten, & Wilking (1990), respectively. Since the H_2 column densities for L1527 and IRAS 15398−3359 in Lup-1 are not reported as far as we know, we did not derive the HCN and HNC abundances for these sources.

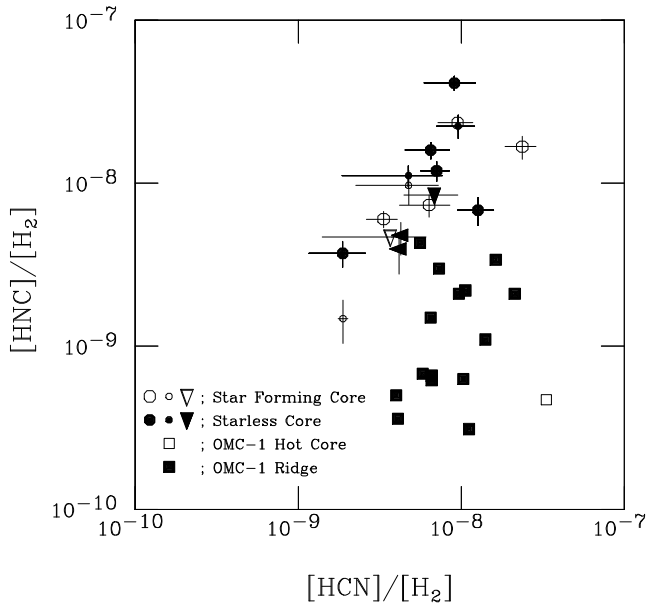

FIG. 3.—Abundance ratios of HCN and HNC relative to H_2 molecules. The filled and open squares represent the abundances of HCN and HNC in ridge and hot core regions of OMC-1, respectively. The symbols for the dark cloud cores are the same as Fig. 2. Data of OMC-1 are taken from Schilke et al. (1992).

The observed abundances of HCN and HNC mostly range from 2×10^{-9} to 2×10^{-8}. We found that the abundances of HCN and HNC are almost constant in dark cloud cores. In addition, it is notable that the abundances of HCN in dark cloud cores are the same as those in OMC-1. On the other hand, the abundances of HNC in dark cloud cores are larger by 1–2 orders of magnitude than those in OMC-1.

According to the pseudo–time-dependent calculations of the new standard model [Lee et al. 1996; $T = 10$ K and $n(H_2) = 10^5$ cm^{-3}], the HCN abundance is predicted to be 7.7×10^{-7}, 1.6×10^{-7}, 4.1×10^{-9}, and 7.2×10^{-10} at $10^{4.5}$, 10^5, $10^{5.5}$ yr, and steady state, respectively, whereas the HNC abundance is 2.7×10^{-7}, 7.8×10^{-8}, 1.5×10^{-9}, and 4.6×10^{-10} for $10^{4.5}$, 10^5, $10^{5.5}$ yr, and steady state, respectively. The observed abundances of HCN and HNC are close to the intermediate values between 10^5 yr and steady state, although the observed and model abundances do not agree well with each other at steady state. Since there is no significant difference in the HCN abundance between the star-forming cores and starless cores, a systematic change in the HCN abundance due to chemical evolution is not apparent in this study. The critical density for the HCN

lines is as high as 10^6 cm^{-3}, so that the lines originate from the densest part of the core. In other words, the lines preferentially trace the advanced stages in chemical evolution from diffuse to dense matter. Because of this, the abundance of HCN in rather constant within a factor of 10 for various sources, regardless of the presence of protostars.

The model predicts the HNC/HCN ratio to be 0.35, 0.49, 0.37, and 0.64 for $10^{4.5}$, 10^5, $10^{5.5}$ yr, and steady state, respectively, which is significantly smaller than the observed value. The ratio is not very sensitive to the cloud ages, and, hence, this discrepancy probably originates from the branching ratio in the dissociative recombination reaction of $HCNH^+$ employed in the model, as described later.

4. DISCUSSION

4.1. *Production Reaction of* HCN *and* HNC *in Dark Cloud Cores*

We observed the $H^{13}CN$ and $HN^{13}C$ lines toward 19 nearby dark cloud cores and found that the HNC/HCN ratio is in the range from 0.54 to 4.5 regardless of whether they are the star-forming cores or the starless cores. Our results are consistent with previous observations (Irvine & Schloerb 1984; Churchwell et al. 1984; Swade 1989a) but provide more reliable values for a number of sources based on observations of optically thin lines.

According to gas-phase chemical models, HCN and HNC are mainly produced by a dissociative recombination reaction of the $HCNH^+$ ion with an electron (Allen, Goddard, & Schaefer 1980; Herbst 1978):

$$HCNH^+ + e \rightarrow \begin{cases} HCN + H & (1a) \\ HNC + H\,. & (1b) \end{cases}$$

In these reactions, the HNC/HCN abundance ratio is predicted to be 0.9 on the basis of the phase-space theory (Herbst 1978). According to the recent quantum chemical calculation, the CN radical should not be produced in the recombination reaction of the $HCNH^+$ ion because simultaneous dissociation of the C-H and the N-H bonds requires two electron excitations and is energetically unfavorable (Shiba et al. 1998). Therefore, we ignored the production channel of the CN radical in reactions (1a) and (1b). Furthermore, Shiba et al. (1998) concluded that HNC is preferentially produced in reaction (1b), in which the production rate of HNC is somewhat larger than that of HCN. From the average HCN/HNC ratio in dark cloud cores, 0.69, the branching ratios of reactions (1a) and (1b) are estimated to be 0.4 and 0.6, respectively (Appendix B), which is consistent with the theoretical considerations (Shiba et al. 1998).

Another possible production reaction of HNC is a dissociative recombination reaction of the H_2NC^+ ion (Allen et al. 1980):

$$H_2NC^+ + e \rightarrow HNC + H\,, \qquad (2)$$

where only HNC is produced. Considering the favorable production of HNC in reaction (1b) and the additional route to produce HNC, the HNC/HCN ratio should be greater than unity, as observed in the present study.

The transitions of $HCNH^+$ toward TMC-1 have been observed (Ziurys, Apponi, & Yoder 1992). However, the H_2NC^+ ion has been detected neither in the laboratory nor in interstellar clouds. Detection of the H_2NC^+ ion would make it possible to understand the production reactions of HCN and HNC in dark cloud cores more quantitatively. In addition, the branching ratio should be determined by laboratory experiments and/or by more detailed calculations in order to construct accurate chemical models of dark cloud cores and cometary comae (Irvine et al. 1998; Hirota et al. 1998).

Our result that the HNC/HCN ratio in star-forming cores is not different from that in starless cores suggest that evaporation of HCN and HNC from dust grains does not contribute significantly to the observed HNC/HCN ratio. This is consistent with the kinetic temperatures of 8 to 15 K for the observed cores (Benson & Myers 1989), which are sufficiently low to inhibit evaporation of HCN and HNC from dust grains. Therefore, the HNC/HCN ratios in dark cloud cores are not affected very much by the activity of low-mass star formation, except for a few sources such as IRAS 16293−2422 (van Dishoeck et al. 1995) and L1157 (Bachiller & Pérez Gutiérrez 1997), where strongly shocked molecular gas exists.

4.2. *The* HNC/HCN *Ratios in OMC-1 and Dark Cloud Cores*

As shown in Figure 3, the HNC/HCN ratios in OMC-1 (Schilke et al. 1992) are much different from those in dark cloud cores. It is evident that the abundance of HCN in OMC-1 is almost the same as that in dark cloud cores. In contrast, the abundance of HNC in OMC-1 is generally lower than the abundances in dark cloud cores. Especially, the HNC abundance in the OMC-1 hot core is 2 orders of magnitude lower than those in dark cloud cores, whereas the HCN abundance is only slightly higher than the typical dark cloud values. Therefore, the HNC/HCN ratio in OMC-1 becomes low because of the low abundance of HNC. It is worth noting that plots of the HCN and HNC abundances are not completely separated in Figure 3 between the groups of dark cloud cores and OMC-1. In other words, the HCN and HNC abundances seem to vary continuously from the dark cloud cores to the OMC-1 hot core. This continuity strongly suggests that the formation chemistry of HCN and HNC in dark cloud cores is similar to that in OMC-1.

van Dishoeck et al. (1995) observed HCN, HNC, and their isotopic species in the $J = 3$–2 and 4–3 transitions toward IRAS 16293−2422 in the dark cloud core L1689N. They obtained an HNC/HCN ratio toward IRAS 16293−2422 of 1/12. In contrast, the HNC/HCN ratio toward the ammonia peak position of L1689N, 100″ east of the *IRAS* position, was derived to be 1.8 ± 0.7 from our $J = 1$–0 observations. According to DCO^+ and NH_3 observations (Wootten & Loren 1987), the kinetic temperature at the ammonia peak seems to be lower than that in the *IRAS* position. Therefore, it is likely that the difference in the HNC/HCN ratio is due to a temperature gradient. van Dishoeck et al. (1995) employed high-J lines whose critical densities are as high as 10^7 cm^{-3}. As a result, they selectively picked up the densest part of the core close to the protostar. In such a part, the kinetic temperature would be 40–80 K (van Dishoeck et al. 1995), and the HNC/HCN ratio toward the *IRAS* position is, consequently, similar to that of OMC-1.

To determine what is responsible for the variation of the HNC/HCN ratio, the relationship between the observed HNC/HCN ratio and kinetic temperature in various sources is shown in Figure 4. This is a diagram similar to

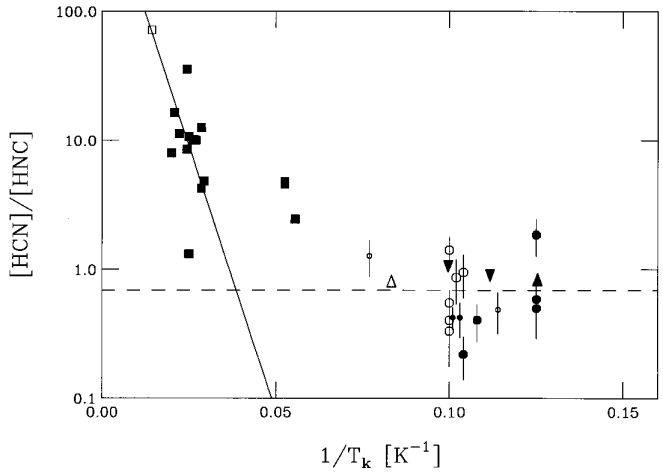

FIG. 4.—Observed HCN/HNC ratio in various sources is plotted against $1/T_k$. The symbols are the same as those of Fig. 3. The OMC-1 data (Schilke et al. 1992) are fitted to the function $[HCN]/[HNC] = A \exp(-\Delta E/T_k)$, where ΔE is the potential barrier, drawn as a solid line. The dashed line is the average HCN/HNC ratio observed in dark cloud cores, 0.69.

that prepared by Irvine, Goldsmith, & Hjalmarson (1987), but the number of data points at low temperatures is much increased in our study. Kinetic temperatures in the OMC-1 hot core and the OMC-1 ridge are 70 K and 20–40 K, respectively (Schilke et al. 1992). As pointed out by Goldsmith et al. (1986) and Schilke et al. (1992), the HNC/HCN ratio in OMC-1 becomes low as the kinetic temperature increases. Since the HCN abundance is almost constant for OMC-1 and dark cloud cores, this result indicates significant depletion of the HNC abundances in high kinetic temperature regions.

The temperature dependence of the HNC/HCN ratio is discussed in Appendix B. The HNC/HCN ratio rapidly decreases as the temperature exceeds the critical temperature of 24 K, which is higher than the kinetic temperature of the dark cloud core. From the slope of plots for $T_k > 24$ K, the activation energy for the depletion process is evaluated to be 190 K. As a destruction process, the following neutral-neutral reactions can be responsible (Schilke et al. 1992; Talbi, Ellinger, & Herbst 1996):

$$HNC + H \rightarrow HCN + H , \quad (3)$$

and

$$HNC + O \rightarrow NH + CO . \quad (4)$$

The activation barrier for the reaction (3) is predicted to be 4.2 kcal mol^{-1} (2000 K) on the basis of quantum chemical calculations (Talbi et al. 1996), which is much different from our observational estimate. On the other hand, no theoretical or experimental studies have been made for the reaction (4). Further laboratory and theoretical studies would be necessary for quantitative identification of the depletion processes.

5. SUMMARY

In this paper, we accurately determined the abundances of HCN and HNC toward 19 dark cloud cores by observing the rare isotopic species, $H^{13}CN$ and $HN^{13}C$. The results are summarized as follows:

1. The column densities of $H^{13}CN$ and $HN^{13}C$ that we obtained are $(0.14–3.7) \times 10^{12}$ cm^{-2} and $(0.24–11) \times 10^{12}$ cm^{-2}, respectively. They are positively correlated, with the correlation coefficient calculated to be 0.72.

2. The largest and smallest values of the HNC/HCN ratio are 4.5 ± 1.2 in L1498 and 0.54 ± 0.33 in L1521E, respectively. The average ratio of all the observed cloud cores is 2.1 ± 1.2. The abundance of HNC is generally higher than that of HCN in dark cloud cores.

3. The abundances of HCN and HNC are not significantly different between the star-forming cores and the starless cores.

4. The present results are consistent with the idea that HCN and HNC are mainly produced in the gas phase through the dissociative recombination reaction of $HCNH^+$. From the observed HNC/HCN ratio, the branching ratio to yield HCN in the dissociative recombination reaction is estimated to be 0.4. This is consistent with the theoretical considerations (Shiba et al. 1998).

5. The HNC/HCN ratios in OMC-1 range from 1 to 1/90 (Schilke et al. 1992), which are smaller than those of dark cloud cores. The abundances of HCN in OMC-1 (Schilke et al. 1992) are almost the same as those in dark cloud cores, whereas the abundance of HNC is depleted in high-temperature regions. The temperature dependence of the HNC/HCN ratio suggests that the HNC may be destroyed by neutral-neutral reactions with an activation barrier of 190 K in the high-temperature regions.

We are grateful to the staff of Nobeyama Radio Observatory for their assistance in observations. We also thank Yoshihiro Osamura of Rikkyo University and Keisaku Ishii of University of Tokyo for useful discussions about the production reactions of HCN and HNC. T. H. thanks the Japan Society for the Promotion of Science for financial support. This study is supported by a Grant-in-Aid from the Ministry of Education, Science, and Culture (05453020 and 07CE2001).

APPENDIX A

OBSERVATIONS OF $C^{34}S$

In order to determine the H_2 densities of the cores, we observed the $J = 1–0$ (48206.95 MHz) and 2–1 (96412.98 MHz) lines of $C^{34}S$ with the 45 m radio telescope of Nobeyama Radio Observatory. Since the dipole moment of CS, 1.97 debye (Mockler & Bird 1955), is larger than that of CO, and since the $C^{34}S$ lines are thought to be optically thin, they are useful for determining the H_2 densities, especially in dense dark cloud cores. We observed the 21 dark cloud cores listed in Table 5. The coordinates of the sources are listed in Tables 2 and 6. The beam sizes (HPBW) are 34″ and 17″ for the $J = 1–0$ and $J = 2–1$ lines, respectively. The beam efficiency is 0.7 for the $J = 1–0$ observations and 0.4 for the $J = 2–1$ observations. The observed spectra of $C^{34}S$ lines toward L1521E are shown in Figure 5.

A method similar to that used for the analysis of HCN and HNC is adopted to calculate the column densities of $C^{34}S$ and the H_2 densities. The kinetic temperatures of the cores are assumed to be 10 K. In the LVG calculations, collision rates for CS

TABLE 5

OBSERVED AND DERIVED PARAMETERS FOR $C^{34}S$

	$J = 1$–0		$J = 2$–1			
SOURCE NAME	T_A^*	Δv (km s^{-1})	T_A^*	Δv (km s^{-1})	$n(H_2)$ (10^5 cm^{-3})	$N(C^{34}S)$ (10^{12} cm^{-2})
B1	1.01	1.07	0.65	1.09	1.6	14.2
L1489	0.20	0.86	<0.18	...	<2.9	<3.0
L1498	0.50	0.38	0.31	0.19	1.4	1.7
L1521B	1.00	0.41	0.70	0.43	1.9	5.6
L1521E	1.61	0.47	0.94	0.55	1.3	12.5
L1551	0.21	1.85	0.26	0.81	13.4	4.2
TMC-2.....	0.44	0.76	0.28	0.38	1.4	2.9
TMC-1(NH_3).....	0.56	0.82	0.43	0.50	2.2	4.5
TMC-1C.....	0.78	0.45	0.22	0.21	0.1	21.8
TMC-1.....	0.97	0.63	0.53	0.50	1.0	7.3
L1544	0.60	0.38	0.27	0.33	0.7	2.8
L134N	0.35	0.71	0.15	0.33	0.4	3.0
L1689N	0.44	1.83	0.37	0.66	2.7	6.8
L43B	0.31	0.41	0.22	0.89	1.7	2.3
L63.....	0.26	0.44	0.31	0.33	7.4	1.5
L778	0.21	0.89	0.12	0.39	1.0	1.5
B335	0.49	0.44	0.24	0.50	0.8	2.8
L1157	0.26	0.36	0.21	0.60	2.4	1.5
L1228	0.17	0.35	0.12	0.51	1.6	0.8
L1221	0.18	1.30	0.16	1.79	2.8	3.3
L1262A	0.21	0.18	0.23	0.51	4.7	1.0

TABLE 6

DARK CLOUD CORES OBSERVED FOR $C^{34}S$

Source Name	α(1950.0)	δ(1950.0)	Distance (pc)
L43B	16 31 39.0	−15 39 27	160
L778	19 24 26.4	23 52 37	420
B335	19 34 33.3	07 27 00	250
L1157.....	20 38 39.6	67 51 33	440
L1228.....	21 00 44.4	78 11 00	200
L1221.....	22 26 37.2	68 45 52	200
L1262A.....	23 23 32.2	74 01 45	200

NOTE.—Units of right ascension are hours, minutes, and seconds, and units of declination are degrees, arcminutes, and arcseconds.

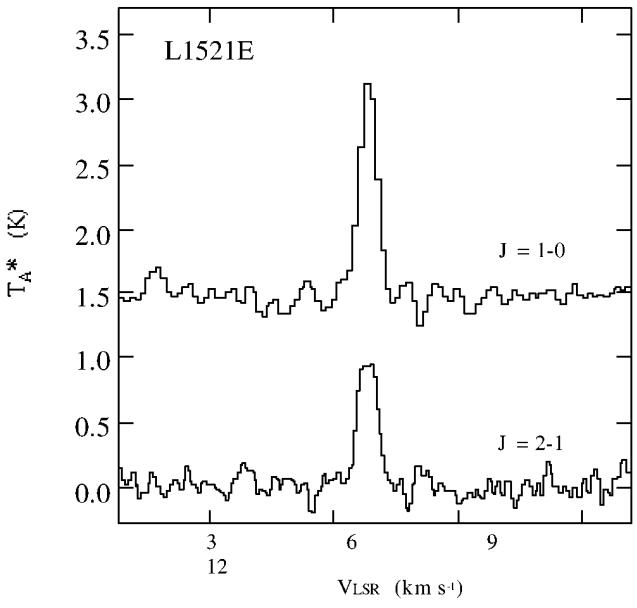

FIG. 5.—Observed spectra of the $C^{34}S$ lines toward L1521E

and H_2 are from Green & Chapman (1978). We ignored the difference in the beam sizes of the two transitions in the analysis, since the emission regions of $C^{34}S$ are sufficiently larger than the beam sizes. Observed line parameters, column densities of $C^{34}S$, and H_2 densities obtained by the LVG calculations are summarized in Table 5.

APPENDIX B

THE TEMPERATURE DEPENDENCE OF HNC/HCN RATIOS

In order to analyze the temperature dependence of the HNC/HCN ratio in a semiquantitative way, we considered the reaction processes shown in Figure 6. We assumed that the $HCNH^+$ ion is produced by the following proton transfer reactions:

$$\mathrm{HCN,\ HNC} + \mathrm{HX}^+ \rightarrow \mathrm{HCNH}^+ + \mathrm{X}\ , \tag{B1}$$

where HX^+ are molecular ions like HCO^+ and H_3O^+.

We are especially interested in the branching ratios of reactions (1a) and (1b) and the destruction mechanism of the HNC molecule in OMC-1. Therefore, for simplicity, we consider the reactions shown in Figure 6 and neglect the other reactions such as the production reactions of $HCNH^+$, other routes of production and destruction of HCN and HNC, and reactions of the H_2NC^+ ion. Considering the reactions (1a), (1b), (3), and (B1), the following rate equations are derived:

$$\frac{d[\mathrm{HCN}]}{dt} = k[\mathrm{HNC}][\mathrm{H}] + \alpha k_r[\mathrm{HCNH}^+][e] - k_p[\mathrm{HCN}][\mathrm{HX}^+]\ , \tag{B2}$$

$$\frac{d[\mathrm{HNC}]}{dt} = -k[\mathrm{HNC}][\mathrm{H}] + (1-\alpha)k_r[\mathrm{HCNH}^+][e] - k_p[\mathrm{HNC}][\mathrm{HX}^+]\ , \tag{B3}$$

and

$$\frac{d[\mathrm{HCNH}^+]}{dt} = -k_r[\mathrm{HCNH}^+][e] + k_p[\mathrm{HCN}][\mathrm{HX}^+] + k_p[\mathrm{HNC}][\mathrm{HX}^+]\ . \tag{B4}$$

Here k_r, k, and k_p are the rate coefficients of the reactions (1a) and (1b), (3), and (B1), respectively. We assume that the branching ratio of the production of HCN by the recombination reaction of $HCNH^+$ (eq. [1a]) is α and that of HNC (eq. [1b]) is $1-\alpha$.

We employ the steady state approximation, and we set the left-hand sides of equations (B2), (B3), and (B4) to zero. Then the HCN/HNC ratio, f, is expressed as

$$f \equiv \frac{[\mathrm{HCN}]}{[\mathrm{HNC}]} = \frac{\alpha}{1-\alpha} + \frac{k[\mathrm{H}]}{(1-\alpha)k_p[\mathrm{HX}^+]}\ . \tag{B5}$$

The rate coefficient of the neutral-neutral reaction (eq. [3]) is assumed to be given in the following form with the activation barrier of E_a:

$$k = k_0 \exp\left[-\left(\frac{E_a}{kT}\right)\right]. \tag{B6}$$

From equations (B5) and (B6), the HCN/HNC ratio is given by

$$f = \frac{\alpha}{1-\alpha} + \frac{k_0[\mathrm{H}]}{(1-\alpha)k_p[\mathrm{HX}^+]} \exp\left[-\left(\frac{E_a}{kT}\right)\right] \tag{B7}$$

$$\sim \begin{cases} \alpha/(1-\alpha)\ ; & T \ll T_c\ , \quad \text{(B8a)} \\ \dfrac{C}{1-\alpha} \exp\left[-\left(\dfrac{E_a}{kT}\right)\right]; & T \gg T_c\ , \quad \text{(B8b)} \end{cases}$$

where the constant C is defined as

$$C \equiv \frac{k_0[\mathrm{H}]}{k_p[\mathrm{HX}^+]}\ , \tag{B9}$$

and T_c is the critical temperature where the constant term is identical to the exponential term in equation (B7).

In dark cloud cores, kT_k is much smaller than E_a, and hence, the second term in equation (B7) can be ignored. From the observed HCN/HNC ratio, we evaluated the branching ratio, α, to be 0.4. For high-temperature regions in OMC-1, the HNC/HCN ratio depends on the kinetic temperature. In this case, the first term in equation (B7) can be neglected, and we derived E_a and C from the observed ratios in OMC-1 using equation (B8b). The activation barrier in equation (B8b) is thus estimated to be 190 K, and the C-coefficient is estimated to be 1020. The first and second terms give equal contributions at $T = 24$ K. Therefore, the ratio is determined by the branching ratio in the recombination reactions (1a) and (1b) below 24 K, whereas it is determined by the neutral-neutral reaction (3) above 24 K.

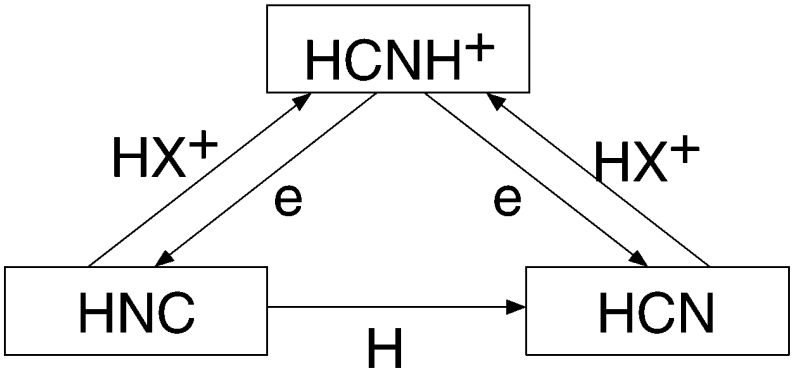

FIG. 6.—Simple chemical network of HCN, HNC, and $HCNH^+$

Here we estimate the order of the C-coefficient in equation (B9). The rate coefficient of the neutral-neutral reaction k_0 and that of the ion-molecular reaction k_p is on the order of 10^{-10} and 10^{-9} cm^3 s^{-1}, respectively. The abundance ratios of $[H]/[H_2]$ and $[HX^+]/[H_2]$ are predicted to be about 10^{-4} and 10^{-8}, respectively (Lee et al. 1996). Thus the C-coefficient in equation (B9) is an order of 10^3. This is consistent with the value obtained in the analysis of the observed data.

REFERENCES

Allen, T. L., Goddard, J. D., & Schaefer III, H. F. 1980, J. Chem. Phys., 73, 3255
Bachiller, R., Menten, K. M., & del Río-Alvarez, S. 1990, A&A, 236, 461
Bachiller, R., & Pérez Gutiérrez, M. 1997, ApJ, 487, L93
Benson, P. J., & Myers, P. C. 1989, ApJS, 71, 89
Bentley, J. A., Huang, C. M., & Wyatt, R. E. 1993, J. Chem. Phys., 98, 5207
Bhattacharya, B. N., & Gordy, W. 1960, Phys. Rev., 119, 144
Blackman, G. L., Brown, R. D., Godfrey, P. D., & Gunn, H. I. 1976, Nature, 261, 395
Butner, H. M., Lada, E. A., & Loren, R. B. 1995, ApJ, 448, 207
Churchwell, E., Nash, A. G., & Walmsley, C. M. 1984, ApJ, 287, 681
Fukui, Y., Sugitani, K., Takaba, H., Iwata, T., Mizuno, A., Ogawa, H., & Kawabata, K. 1986, ApJ, 311, L85
Goldreich, P., & Kwan, J. 1974, ApJ, 189, 441
Goldsmith, P. F., Irvine, W. M., Hjalmarson, Å., & Elldér, J. 1986, ApJ, 310, 383
Goldsmith, P. F., Langer, W. D., Ellder, J., Irvine, W., & Kollberg, E. 1981, ApJ, 249, 524
Green, S., & Chapman, S. 1978, ApJS, 37, 169
Green, S., & Thaddeus, P. 1974, ApJ, 191, 653
Harju, J. 1989, A&A, 219, 293
Herbst, E. 1978, ApJ, 222, 508
Heyer, M. H., Snell, R. L., Goldsmith, P. F., & Myers, P. C. 1987, ApJ, 321, 370
Hirota, T., Yamamoto, S., Kawaguchi, K., Sakamoto, A., & Ukita, N. 1998, ApJ, submitted
Irvine, W. M., Goldsmith, P. F., & Hjalmarson, Å. 1987, in Astrophysics and Space Science Library, Vol. 134, Interstellar Processes, ed. D. J. Hollenbach & H. A. Thronson, Jr. (Dordrecht: Reidel), 561
Irvine, W. M., & Schloerb, F. P. 1984, ApJ, 282, 516
Irvine, W. M., et al. 1998, Faraday Disc., 109, in press
Langer, W. D., & Penzias, A. A. 1993, ApJ, 408, 539
Lee, H. -H., Bettens, R. P. A., & Herbst, E. 1996, A&AS , 119, 111
Loren, R. B., Wootten, A., & Wilking, B. A. 1990, ApJ, 365, 269
Lovas, F. J., Snyder, L. E., & Johanson, D. R. 1979, ApJS, 41, 451
Mangum, J. G., Rood, R. T., Wadiak, E. J., & Wilson, T. L. 1988, ApJ, 334, 182
Mockler, R. C., & Bird, G. R. 1955, Phys. Rev., 98, 1837
Monteiro, T. S., & Stutzki, J. 1986, MNRAS, 221, 33P
Myers, P. C., Bachiller, R., Caselli, P., Fuller, G. A., Mardones, D., Tafalla, M., & Wilner, D. J. 1995, ApJ, 449, L65
Myers, P. C., Heyer, M., Snell, R. L., & Goldsmith, P. F. 1988, ApJ, 324, 907
Myers, P. C., Linke, R. A., & Benson, P. J. 1983, ApJ, 264, 517
Myers, P. C., Mardones, D., Tafalla, M., Williams, J. P., & Wilner, D. J. 1996, ApJ, 465, L133
Parker, N. D., Padman, R., & Scott, P. F. 1991, MNRAS, 252, 442
Pratap, P., Dickens, J. E., Snell, R. L., Miralles, M. P., Bergin, E. A., Irvine, W. M., & Schloerb, F. P. 1997, ApJ, 486, 862
Schilke, P., Walmsley, C. M., Pineau des Forêts, G., Roueff, E., Flower, D. R., & Guilloteau, S. 1992, A&A, 256, 595
Schinke, R., Engel, V., Buck, U., Meyer, H., & Diercksen, G. H. F. 1985, ApJ, 299, 939
Shiba, Y., Hirano, T., Nagashima, U., & Ishii, K. 1998, J. Chem. Phys., 108, 698
Snell, R. L., Loren, R. B., & Plambeck, R. L. 1980, ApJ, 239, L17
Suzuki, H., Yamamoto, S., Ohishi, M., Kaifu, N., Ishikawa, S., Hirahara, Y., & Takano, S. 1992, ApJ, 392, 551
Swade, D. A. 1989a, ApJ, 345, 828
———. 1989b, ApJS, 71, 219
Tachihara, K., Dobashi, K., Mizuno, A., Ogawa, H., & Fukui, Y. 1996, PASJ, 48, 489
Talbi, D., Ellinger, Y., & Herbst, E. 1996, A&A, 314, 688
Ungerechts, H., Bergin, E. A., Goldsmith, P. F., Irvine, W. M., Schloerb, F. P., & Snell, R. L. 1997, ApJ, 482, 245
van Dishoeck, E. F., Blake, G. A., Jansen, D. J., & Groesbeck, T. D. 1995, ApJ, 447, 760
Wootten, A., & Loren, R. B. 1987, ApJ, 317, 220
Ziurys, L. M., Apponi, A. J., & Yoder, J. T. 1992, ApJ, 397, L123